Physical Features and Parameters Calculations of a Hall Thruster

IEPC-2011-002

Presented at the 32nd International Electric Propulsion Conference,
Wiesbaden • Germany
September 11 – 15, 2011

M.H.Moghimi[1]
M.Sc. in Aerospace Engineering, Sharif University of Technology, Tehran, 1581955711, Iran

Abstract: The engineering method of the Hall thruster integral parameters calculating basing on the experimental materials is studied. It permits to calculate the Hall thruster integral parameters as a dependence of an accelerating channel geometry size, value of working medium flow rate and its kind, and the discharge voltage for the optimal working regime. The process will begin by criteria for the operation of a hall thruster by using the ionization layer formula and make a relation between the mean diameter, and mass flow rate of Xenon beside the other parameters. Then jet power of the exhausted ion flow will be calculated. This power will be used for calculation of the acceleration voltage in the acceleration layer. To this point many of the geometrical dimensions were calculated. After these calculations a criteria must be defined for the operation time of the thruster. This criterion specified as the erosion rate of the wall of the acceleration channel. The method has been used to design a hall thruster with operating characteristics similar to SPT-100.

Nomenclature

B, B_r	=	magnetic induction, and its radial component respectively
d	=	accelerating channel mean diameter
w, δ_w	=	accelerating channel width, and wall thickness respectively
L, L_{ac}, L_i	=	channel length, acceleration layer length, and ionization layer length respectively
E, E_z	=	electric field, and its axial component respectively
h_c	=	cycloid height, $2mE_z/eB_r^2$
j, j_z, j_H	=	current density, its axial component, and electron Hall current density respectively
e, m, n_e	=	electron charge, electron mass, and electron density respectively
M	=	ion and atom mass
K_B	=	Boltzmann constant
$\dot{m}$	=	total mass flow rate
$\dot{m}_a, \dot{m}_c$	=	mass flow rate through the accelerating channel, and mass flow rate through the cathode
I_d	=	discharge current
$I_{\dot{m}}$	=	current corresponding to mass flow rate through the accelerating channel, $(\dot{m}_a/M)e$
U_d, φ_i, Φ	=	discharge voltage, gas atom ionization potential, and magnetic flux respectively
V, T_e, T_i	=	velocity, electron temperature, and ion temperature respectively
ν, τ, t	=	collision frequency, time between electron collisions, and time respectively
η	=	efficiency
ω	=	electron cyclotron frequency, (eB/m)
σ_i	=	ionization cross section
$\mu_e, \mu_{e\perp}$	=	electron mobility, and electron mobility perpendicular to magnetic field
r_{Le}, r_{Li}	=	electron Larmor radius, and ion Larmor radius respectively

[1] M.Sc. in Aerospace Engineering, Aerospace Engineering Department, m_moghimi@alum.sharif.edu.

I. Introduction

Electric propulsion systems (EPSs) for spacecraft maneuvering and orbit control are the technology for improving spacecraft performance levels and increasing their capabilities because of significantly higher specific impulses of EPSs in comparison with chemical propulsion systems. The study of Hall thrusters (or stationary plasma thrusters) was initiated independently in the USSR and the US at the end of 1950s. The efforts in the USSR and the US from the beginning of 1960s to the end of this decade led to Hall thrusters with efficiency about 50% and a little above this value with the design features similar to present designs like: external applied magnetic field, external sources of electron, and steady state operation in the moderate power levels. However, because of the slower progress in the space electrical power plants only a small number of electric thrusters with relatively low power consumption were applied for space missions. One of these electrical space propulsion systems was hall thruster, a thruster with relatively simple geometry in comparison with the other thrusters like ion thruster. Meteor satellite with the first onboard Hall thruster (Eol-1), as shown in Fig. 1, was launched to space in December 1971 and the first Hall thruster space test was successfully realized by soviet's scientific centers like: All-Russia Scientific and Research Institute of Electro-Mechanic (VNIIEM), and Experimental Design Bureau "Fakel".[1]

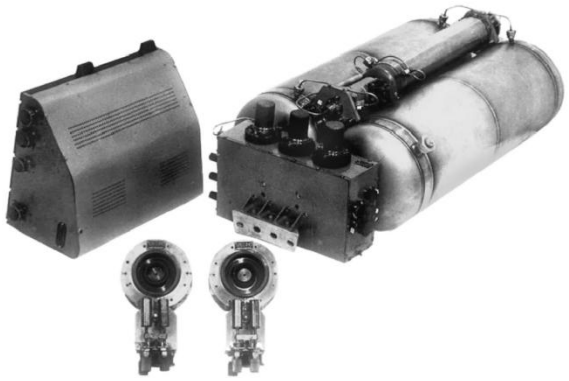

Figure 1. The "Eol-1" Propulsion system parts from Ref. 1.

Since those days to the present time the propulsion subsystems based on this thruster has widely used onboard western and eastern satellites. In addition it has described in Ref. 2 that this thruster has required capabilities for interplanetary missions like spacecraft Phobos-Grunt as a mars orbiter and Lander whose aim is to deliver soil samples from Phobos. Regarding to the importance of this issue and also scientists' theoretical and experimental studies on Hall thruster's physics and performance for more than 50 years, it seems useful to review the physical features and implementation of a theoretical method beside the experimental data to achieve a simple algorithm design for these kind of thrusters. It is necessary to add that this investigation is based on a type of Hall thruster which categorized in eastern literature as stationary plasma thruster.

II. Main Physical Processes in Hall Thruster

In this section we proceed by reviewing some operating principles of a Hall thruster then make a relation between the thruster geometry, external applied magnetic field, and the discharge voltage. At the end we discussed the erosion process of the acceleration channel wall briefly to achieve a criterion for the operational time of the thruster.

A. Schematic Diagram of a Hall Thruster

Hall Thrusters are relatively simple devices consisting of a cylindrical channel with an interior anode, a magnetic circuit that generates a primary radial magnetic field across the channel, and a cathode external to the channel. Hall-effect thrusters (HETs), stationary plasma thrusters (SPTs), and magnetic-layer thrusters are all names for essentially the same device that is characterized by the use of a dielectric insulating wall in the plasma channel, as illustrated in Fig. 2. The wall is typically manufactured from ceramics like: boron nitride (BN) or borosil (BN-SiO_2) in flight thrusters, and also sometimes alumina (Al_2O_3) in laboratory thrusters.

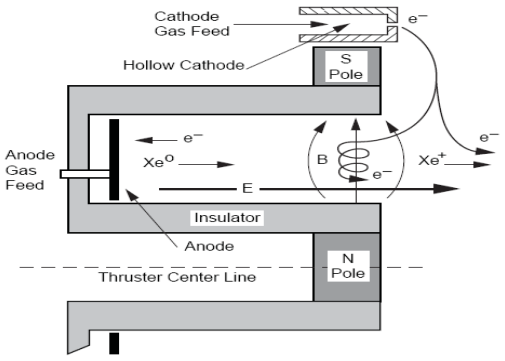

Figure 2. The Hall thruster cross-section schematic from Ref. 3.

The ceramic wall plays an important role in the discharge. The collisions of electrons and ions with the wall generate low energy secondary electrons. These secondary electrons tend to keep the electron temperature low in the discharge plasma. This low electron temperature in return results in a more extended and gradual acceleration process.

The efficient operation of Hall thrusters is based upon the reduced mobility of electrons across the magnetic field. In this thruster the radial magnetic field along the channel is produced between an inner ferromagnetic core and outer ferromagnetic ring. The distribution of the radial magnetic field and the resulting electric field distribution, together with the motions of electrons and ions are shown in Fig. 3.

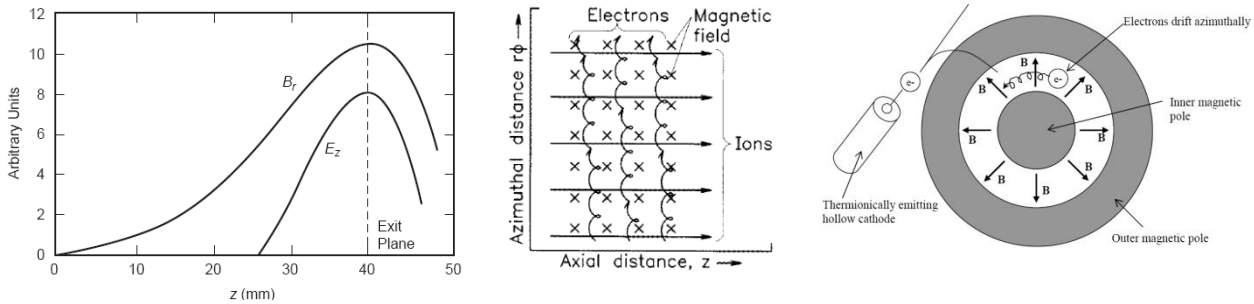

Figure 3. From left to right respectively: magnetic field and electric field distribution along the channel, motion of electrons and ions, and the front view of electron motion in the channel.

The axial variation in the strength of the radial magnetic field has a bell-shaped distribution, reaching a maximum near the exit plane and decreasing both near the anode. Also in the resulting electric field distribution most of the potential variation is near the region of the maximum magnetic field strength. This strength must satisfy the following conditions:

$$r_{Le} \ll w \ll r_{Li} \tag{1}$$

This relation shows that in electron Hall thruster the confinement of electron is the key physical feature for the operation of the propulsion system. This field strength is such that the heavy ions experience negligible influence due to the magnetic field, while the trajectory of the much lighter electrons is significantly affected. As the electrons proceed from the cathode to the anode due to the axial electric field the magnetic field configuration results in an $\boldsymbol{E} \times \boldsymbol{B}$ drift (Hall current) in the azimuthal direction impeding their progress to the anode. The electrons are effectively trapped in a closed drift azimuthal orbit with only collisions between electrons, ions, neutrals particles, and the channel walls permitting a slow diffusion back to the anode. Due to the highly suppressed axial mobility of the electrons the plasma can support a very large axial electric field with a potential difference close to the applied voltage between the electrodes. Propellant atoms (usually Xenon) are introduced to the discharge volume through small holes in the annular anode. Through collisions with the trapped electrons, these atoms are ionized shortly after entering the discharge; the ionized propellant is then accelerated through the large axial electric field producing a reactive thrust.

In particular, to optimize the ionization process it is necessary to optimize the quantity the electrons going through the channel and coupling energy from the electric field. Ideally, this energy is equal to the value necessary for ionization of the full gas flow, and so it is necessary to control the electron current through the channel. In other words, confinement of electrons in a thin region to make a layer for effective collision processes with the atoms is the physics which must be considered.

The calculation of electron Hall current density j_H and electron longitudinal current density j_{ez} allowed one to reach the effective electron Hall parameter $(\omega\tau)_{eff} = j_H / j_{ez}$ which could be a criterion for high confinement of electron and high probability of effective collisions. The measurements showed that this parameter is about 200-300 in a zone where the electron Hall current is mainly located and where the magnetic field is high enough.

The frequency of the electron collisions with the atoms and walls is significantly higher than for electron-ion collisions in the channel. Therefore, it is possible to use the classical conductivity in plasma at least in the part of the channel with high magnetic field induction values, where the acceleration layer is located. For the axisymmetrical channel configuration, where magnetic field B is directed along the radius (x axis), the electric field is directed mainly along the z axis (parallel to the thruster axis in Fig. 2) and the y axis is directed along the azimuthal direction of the channel it is possible to write the electron momentum equation to obtain a relation between the electron Hall current density and electron longitudinal current density as below;

$$mn_e \left[\frac{\partial \boldsymbol{V}_e}{\partial t} + (\boldsymbol{V}_e.\nabla)\boldsymbol{V}_e\right] = -\mathrm{e}n_e(\boldsymbol{E} + \boldsymbol{V}_e \times \boldsymbol{B}) - \nabla p_e - (mn_e\nu_e)\boldsymbol{V}_e \tag{2}$$

Where $\boldsymbol{V}_e$, $p_e = n_e K T_e$, ν_e are electron density, velocity vector, electron pressure, and collision frequency respectively. Neglecting the inertia, the axial electron current density is related to the Hall parameter through the steady state, one dimensional electron momentum equation:

$$0 = en_e E_z + \underbrace{(-en_e V_{e\theta})}_{\mathrm{j_H}} B_r + \frac{\partial p_e}{\partial z} + (mn_e\nu_e)\mathrm{V_{ez}} \tag{3}$$

$$0 = en_e E_z + \mathrm{j}_{e\theta} B_r + \frac{\partial p_e}{\partial z} + (mn_e\nu_e)\mathrm{V_{ez}} \tag{4}$$

Where $V_{e\theta}, j_{e\theta}$ are electron azimuthal velocity, and electron azimuthal current density respectively. In addition neglecting the electron inertia in the azimuthal electron momentum equation yields a relationship between the azimuthal and axial current densities and the electron Hall parameter:

$$0 = \underbrace{-en_e V_{ez}}_{\mathrm{j_{ez}}} B_r - (mn_e\nu_e)\mathrm{V_{e\theta}} \tag{5}$$

$$\frac{j_{e\theta}}{\mathrm{j_{ez}}} = -\frac{B_r e n_e}{m n_e \nu_e} = -\frac{B_r e}{m\nu_e} \xrightarrow{\omega=\frac{eB_r}{m}} \frac{j_{e\theta}}{\mathrm{j_{ez}}} = -\frac{\omega}{\nu_e} = -(\omega\tau)_e \tag{6}$$

By using Eqs. (4), and (6) and definition of electron mobility μ_e electron axial current and consequently electron azimuthal current could be obtained:

$$0 = en_e E_z - \mathrm{j_{ez}}(\omega\tau)_e B_r + \frac{\partial p_e}{\partial z} - (m\nu_e)\frac{j_{ez}}{e} \tag{7}$$

$$\mathrm{j_{ez}}\left[(\omega\tau)_e B_r + \frac{m\nu_e}{e}\right] = en_e E_z + \frac{\partial p_e}{\partial z} \xrightarrow{\mu_e=\frac{e}{m\nu_e}} \mathrm{j_{ez}}\left[(\omega\tau)_e B_r + \frac{1}{\mu_e}\right] = en_e E_z + \frac{\partial p_e}{\partial z} \tag{8}$$

$$\mathrm{j_{ez}} = \frac{\mu_e}{1+(\omega\tau)_e^2}\left(en_e E_z + \frac{\partial p_e}{\partial z}\right) \tag{9}$$

Where $\mu_{e\perp} = \frac{\mu_e}{1+(\omega\tau)_e^2}$. Consequently the electron azimuthal current is:

$$\mathrm{j_{e\theta}} = \frac{-(\omega\tau)_e \mu_e}{1+(\omega\tau)_e^2}\left(en_e E_z + \frac{\partial p_e}{\partial z}\right) \tag{10}$$

Taking onto account $(\omega\tau)_e \gg 1$, it is possible to obtain:

$$\mathrm{j_{ez}} \approx -\frac{1}{(\omega\tau)_e} j_{e\theta} \tag{11}$$

Therefore, electron movement could be interpreted as the so-called electron drift in crossed electric and magnetic fields. The term $en_e E_z + \frac{\partial p_e}{\partial z}$ in Eqs. (9), and (10) shows the electron heating by an electric. At the kinetic level, the collisions of the drifting electrons in the azimuthal direction cause their scattering by the other particles and walls and the transformation of their drift velocity component to the thermal velocity. Thus, collisions of electrons cause

electron directed energy dissipation and the electric field repairs the drift velocity, adding energy to the electrons. This process gives the averaged shift of electrons in the axial direction and to the anode at each collision with heavy particles and walls and explains both the electron transport across the magnetic field in the accelerating layer and the energy transfer from the electric field to the electrons. In Hall thrusters maximizing the ion current to the discharge current is a criterion for optimizing the magnetic field. Simply it could be showed that if the ion to electron current ratio will be in its maximum condition (Eq. (11) describes this issue in other words) the so-called ion to discharge current ratio will be in its optimum operating condition.

B. Ionization Layer and Hall Thruster Operation Criterion

The neutral gas injected from the anode region will be ionized by entering the plasma discharge in the crossed field ionization region. Consider a neutral gas atom at a velocity V_{az} incident on plasma of a density n_e , electron temperature T_e , and thickness L_i . The density of the neutral gas will decrease with time due to ionization:

$$\frac{dn_a}{dt} = -n_a n_e \langle \sigma_i V_e \rangle , \tag{12}$$

Where $\langle \sigma_i V_e \rangle$ is the ionization reaction rate coefficient for Maxwellian electrons. The flux of neutrals incident on the plasma is

$$\Gamma_a = n_a V_{az} , \tag{13}$$

and the neutral velocity is $V_{az} = \frac{dz}{dt}$. Eq. (12) then becomes

$$\frac{\mathrm{d}\Gamma_a}{\Gamma_a} = -\frac{n_e \langle \sigma_i V_e \rangle}{V_{az}} dz . \tag{14}$$

This equation has the solution of

$$\Gamma_a(z) = \Gamma(0) e^{\frac{-z}{\lambda_i}} , \tag{15}$$

where $\Gamma(0)$ is the incident flux on the ionization region and the ionization mean free path λ_i is given by

$$\lambda_i = \frac{V_{az}}{n_e \langle \sigma_i V_e \rangle} . \tag{16}$$

Therefore, the ionization mean free path depends on the neutral velocity, which determines the atom spends in the plasma thickness prior to a collision. The mean free path also varies inversely with the electron density because a higher number of the electrons in the slab will increase the probability of one of them encountering the neutral atom. The percentage of the neutrals existing in the plasma of length L_i that are ionized is

$$\frac{\Gamma_{exit}}{\Gamma_{incident}} = 1 - e^{\frac{-L_i}{\lambda_i}} . \tag{17}$$

It is clear from Eq. (17), in order to have 95% of the incident neutral flux on the plasma ionized before it leaves the plasma, the plasma thickness must be at least three times the ionization mean free path.

With assumption the quasi neutrality of the plasma the electron density will be calculated by using: [5]

$$n_e \cong n_i \cong \frac{\dot{m}_a}{MV_iS_{ch}} \; ; \tag{18}$$

where V_i, and S_{ch} are ion velocity and channel cross section area respectively. In Eq. (18), $V_i = \sqrt{\frac{2e\Delta U_{iz}}{M}}$ and ΔU_{iz} is the potential difference along the ionization layer. This potential difference is about $(2.5, \dots, 3)\varphi_i$; [6,7,8,9] φ_i is the first ionization potential of the Xenon atom; and its value is 12.1 eV. In addition, it must be note that the propellant atoms after heating through the anode will be injected in the channel. The temperature of the atom T_a is about 800K to 1000K for discharge voltage interval of 150 to 350 volts. [7,8,9] The term $\langle \sigma_i V_e \rangle$ is also a function of electron temperature and the electron temperature in the ionization layer for the discharge voltage of 150 to 900 volts will change from 10 to 20 eV; [7,8,9] and the relation between these two parameters are linear. There is a relation for the term $\langle \sigma_i V_e \rangle$ as below: [3]

$$\begin{aligned} \langle \sigma_i V_e \rangle \cong \langle \sigma_i \rangle \bar{V}_e &= 10^{-20}\left[(3.97 + 0.643T_{eV} - 0.0368T_{eV}^2)e^{-12.127/T_{eV}}\right]\left(\frac{8eT_{eV}}{\pi m}\right)^{1/2}, T_{eV} < 5eV \, , \\ \langle \sigma_i V_e \rangle \cong \langle \sigma_i \rangle \bar{V}_e &= 10^{-20}\left[-(1.031 \times 10^{-4})T_{eV}^2 + 6.386e^{-12.127/T_{eV}}\right]\left(\frac{8eT_{eV}}{\pi m}\right)^{1/2}, T_{eV} > 5eV \, . \end{aligned} \tag{19}$$

It is clear to reach high ionization efficiency below condition must be satisfied; [6]

$$\lambda_i = K_\lambda . L_{ac} \, , K_\lambda \ll 1 \, . \tag{20}$$

The channel cross section area is:

$$S_{ch} = \frac{\pi d_{ouc}^2}{4} - \frac{\pi d_{inc}^2}{4} = \pi\left(\frac{d_{ouc} - d_{inc}}{2}\right)\left(\frac{d_{ouc} + d_{inc}}{2}\right) = \pi w d \, . \tag{21}$$

Where d_{ouc} , and d_{inc} are outer channel diameter, and inner channel diameter respectively.

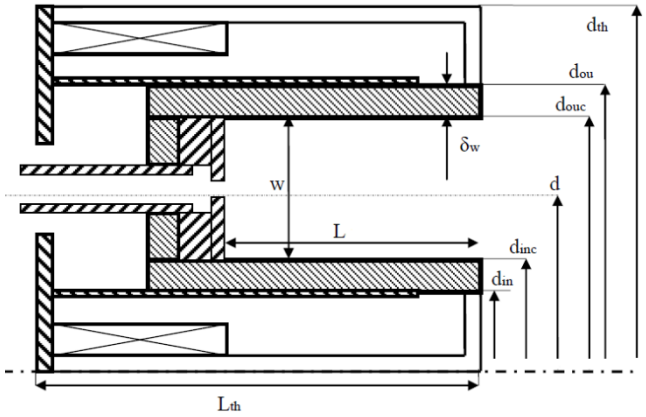

Figure 4. A schematic view of a Hall thruster with the required dimensions.

By using Eqs. (18), and (20) it is possible to reach a relation between the propellant mass flow rate and the channel mean diameter as mentioned below: [5]

$$\frac{\dot{m}_a}{\pi d} \geq \xi \frac{\mathrm{M} V_i V_a}{\langle \sigma_i V_e \rangle}. \tag{22}$$

Eq. (22) is the restriction for the flow rate density through the accelerating channel. In addition, the longitudinal component of atomic velocity V_{az} is about $\xi = (0.25, \dots, 0.5)$ of thermal atomic velocity ($V_a = \sqrt{\frac{8K_B T_a}{\pi M}}$).[5]

C. A Relation between Magnetic Field, Accelerating Channel Width, and Discharge Voltage

At first it is required to write the production rate of the particles per unit area in the acceleration layer to obtain a relation between three parameters known as magnetic field, accelerating channel width, and discharge voltage.

$$Q \cong \mathrm{L}^*_{\mathrm{ac}}\, \mathrm{n_e} \langle \sigma_i V_e \rangle n_a = \mathrm{L}^*_{\mathrm{ac}}\, \mathrm{n_e}\, \mathrm{v_{iz}} \tag{23}$$

Where ν_{iz} , L^*_{ac} are ionization frequency, and length of self-consistent acceleration layer. Also it is possible to write Q with electron axial current density as below:

$$Q = \frac{j_{ez}}{e} = \frac{e n_e V_{e\perp}}{e} = \frac{e n_e \mu_{e\perp} E_z}{e}. \tag{24}$$

The perpendicular electron mobility could be rewritten in the form

$$\mu_{e\perp} = \frac{\mu_e}{1 + (\omega\tau)_e^2} \xrightarrow{(\omega\tau)_e \gg 1} \mu_{e\perp} = \frac{\mu_e}{(\omega\tau)_e^2} = \frac{e/m\nu_e}{(\omega\tau)_e^2} = \frac{1}{B_r} \frac{1}{(\omega\tau)_e}. \tag{25}$$

By putting Eq. (25) in Eq. (24) Q can have the following form:

$$Q = \frac{e n_e \mu_{e\perp} E_z}{e} = n_e \left(\frac{U_d}{L^*_{ac}}\right) \frac{1}{B_r} \frac{1}{(\omega\tau)_e}. \tag{26}$$

By equating Eq. (23) and (26) the length of self-consistent acceleration layer is:

$$L^*_{ac} = \sqrt{\frac{m U_d}{e B_r^2} \frac{\nu_e}{\nu_{iz}}}. \tag{27}$$

It should be note that the length of self-consistent acceleration layer determined in Eq. (27) by the equilibrium between the ionization rate in the acceleration layer and the removal rate of the electrons from this layer by electron conductivity. The frequency ratio $\sqrt{\frac{\nu_e}{\nu_{iz}}}$ could be estimated from Fig. 5 which is a graph of $\sqrt{\frac{\nu_e}{\nu_{iz}}}$ versus electrons energies.

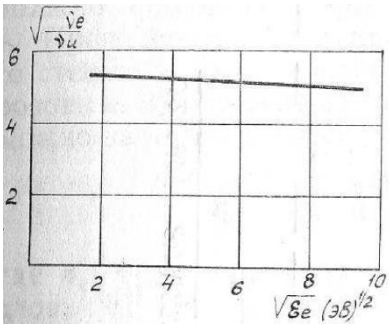

Figure 5. Frequency ratio versus electron energy from Ref. 9.

It is possible to write the axial gradient of the electron axial current density as below:

$$\frac{dj_{ez}}{dz} = j_{ez}\frac{\langle\sigma_i V_e\rangle}{V_{ez}}n_a \rightarrow \frac{dj_{ez}}{j_{ez}} = \frac{\langle\sigma_i V_e\rangle}{V_{ez}}n_a dz\,. \tag{28}$$

By using Eq. (26) and with previous assumption $(\omega\tau)_e \gg 1$, V_{ez} can have the following form:

$$V_{ez} = \frac{E_z}{(\omega\tau)_e B_r}. \tag{29}$$

By putting Eq. (29) in Eq. (28) it is possible to obtain the following relation:

$$\frac{dj_{ez}}{j_{ez}} = \frac{\langle\sigma_i V_e\rangle n_a}{\frac{E}{B_r}\frac{m}{eB_r}\nu_e}dz = \frac{\nu_{iz}}{\nu_e}\frac{2}{h_c}dz\,, \tag{30}$$

$$dlnj_{ez} = \frac{\nu_{iz}}{\nu_e}\frac{2}{h_c}dz = \alpha dz\,. \tag{31}$$

The solution of Eq. (31) is:

$$j_{ea} = j_{eo}\ exp\left[\int_0^{L^*_{ac}} \alpha dz\right] = j_{eo}\ exp[\langle\alpha\rangle L^*_{ac}]\,. \tag{32}$$

In Eq. (32) j_{eo} is the electron current density at the exit of the acceleration channel or at the cathode side of acceleration layer and j_{ea} is electron current density at the anode side of the acceleration layer. Also $\langle\alpha\rangle$ is the mean number of collisions led to ionization when an electron passing axial unit length of the acceleration layer. Furthermore, the ions current density at the exit of the acceleration layer could be shown as below:

$$j_{io} = j_{eo}\ [exp(\langle\alpha\rangle L^*_{ac}) - 1]\ . \tag{33}$$

It is possible to suppose that

$$j_{ea} = j_d = \frac{I_d}{S_{ch}}\ . \tag{34}$$

Therefore, from relations (27), (32), (33), and (34) the following form obtained:

$$\frac{j_{io}}{j_d} = \frac{exp(\langle\alpha\rangle L^*_{ac}) - 1}{exp(\langle\alpha\rangle L^*_{ac})}\ . \tag{35}$$

Taking into account Eqs. (25), (27), (31), (32), (33), and (35) it is possible to obtained in a first approximation,

$$\frac{j_{io}}{j_d} \approx constant\ . \tag{36}$$

Because under optimized operation modes with high enough voltages and mass flow rates:

$$j_{io} \approx j_{\dot{m}} = \frac{e\dot{m}_a}{MS_{ch}} \ . \tag{37}$$

Then it is possible to write that $\frac{j_d}{j_{\dot{m}}} \approx const.$; [6] the value of $\frac{I_d}{I_{\dot{m}}}$ ratio is 1.2 to 1.4. [9] This conclusion is confirmed in a first approximation by the experimental data which has been shown in Fig. 6.

By some algebraic calculations the thruster propellant usage efficiency $\eta_m = \frac{\dot{m}_i}{\dot{m}_p}$ which is the ratio of ion mass flow rate to the total propellant mass flow rate could be shown as the form of Eq. (38).

In Eq. (38) the term V_{io} is the ion velocity at the cathode side of acceleration layer. Also the term ν_W is the electron-wall collision frequency which is given in Ref. 9 as the form of Eq. (39);

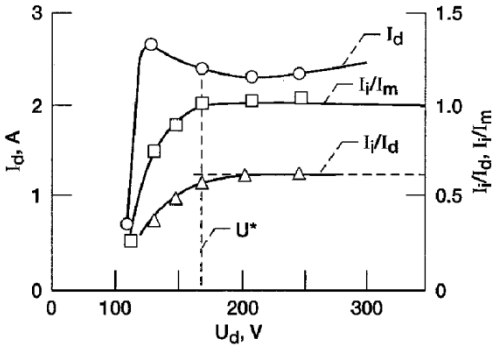

Figure 6. Voltage-Current characteristics of SPT from Ref. 6.

$$\eta_m = 1 - \frac{\nu_W}{\nu_{ea}(\dot{m}_a)}\left[\frac{2V_{io}}{h_c(e^{\langle\alpha\rangle L^*_{ac}} - 1)\nu_W} - 1\right] , \tag{38}$$

$$\nu_W \cong K_W \frac{V_{ea}}{w} . \tag{39}$$

In Eq. (39) V_{ea} is the electron velocity at the anode side of the acceleration layer. The coefficient K_W is given in Ref. 9 as the below form:

$$K_W = \frac{(n_e V_e)_W}{(n_e V_e)_o}\frac{\Delta V_W}{V_o} \ . \tag{40}$$

Where $(n_e V_e)_W$, $(n_e V_e)_o$, ΔV_W, and V_o are number of electrons per square meter collide with wall in a second, number of electrons per square meter in the center of the plasma, electron velocity difference at the wall, and velocity of the electron at the center of the plasma respectively. The ratio $\frac{(n_e V_e)_W}{(n_e V_e)_o}$ is about 0.1 from Ref. 9 and is for the case that the potential differences in the near wall sheath 2.5 times the electron temperature. In addition the term $\frac{\Delta V_W}{V_o}$ in Ref. 9 introduced as the following form:

$$\frac{\Delta V_W}{V_o} = 1 - \cos 2\alpha_s \ . \tag{41}$$

Where α_s is the roughness angle shown in Fig. 9 for the saw-liked wall profile.

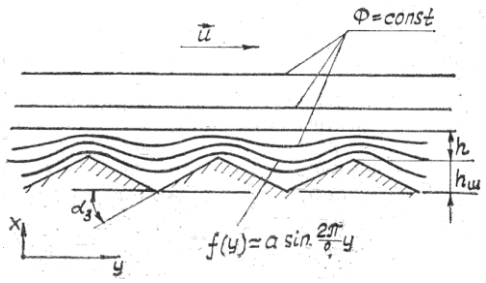

Figure 7. Microscopic view of electron trajectories from Ref. 9.

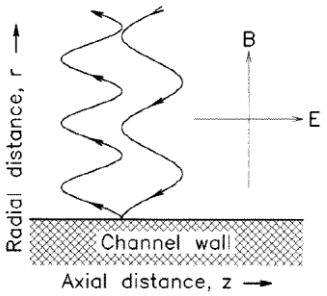

Figure 8. Macroscopic view of electron trajectories from Ref. 4.

The value of α_s in Ref. 9 is about 20 to 24 degree. Now the required tools are ready to reach the relation between the channel width, magnetic field, and the discharge voltage. To obtain the maximum propellant usage efficiency it is required to have the term in bracket in Eq. (38) near to zero.

$$h_c \cong \frac{2V_{io}}{(e^{\langle\alpha\rangle L^*_{ac}}-1)\nu_W} \rightarrow \frac{2mE_z}{eB_r^2} \cong \frac{2V_{io}}{(e^{\langle\alpha\rangle L^*_{ac}}-1)\nu_W} \xrightarrow{E_z=\frac{U_d}{L^*_{ac}}} m\frac{U_d}{L^*_{ac}}\frac{1}{eB_r^2} \cong \frac{V_{io}}{(e^{\langle\alpha\rangle L^*_{ac}}-1)\nu_W}$$

$$\xrightarrow{L^*_{ac}=\sqrt{\frac{mU_d}{eB_r^2}\frac{\nu_e}{\nu_{iz}}}} \frac{mU_d}{eB_r^2\sqrt{\frac{mU_d}{eB_r^2}\frac{\nu_e}{\nu_{iz}}}} \cong \frac{\sqrt{\frac{2eU_d}{M}}}{(e^{\langle\alpha\rangle L^*_{ac}}-1)\nu_W} \rightarrow \sqrt{\frac{mU_d}{eB_r^2}\frac{\nu_{iz}}{\nu_e}} \cong \frac{\sqrt{\frac{2eU_d}{M}}}{(e^{\langle\alpha\rangle L^*_{ac}}-1)\nu_W}$$

$$\xrightarrow{\nu_W \cong K_W\frac{V_{ea}}{w}} \sqrt{\frac{mU_d}{eB_r^2}\frac{\nu_{iz}}{\nu_e}} \cong \frac{\sqrt{\frac{2eU_d}{M}}}{K_W\frac{V_{ea}}{w}(e^{\langle\alpha\rangle L^*_{ac}}-1)} \xrightarrow{V_{ea}=\sqrt{\frac{2eU_d}{m}}} \frac{1}{w}\sqrt{\frac{mU_d}{eB_r^2}\frac{\nu_{iz}}{\nu_e}} \cong \frac{\sqrt{\frac{2eU_d}{M}}}{K_W\sqrt{\frac{2eU_d}{m}}(e^{\langle\alpha\rangle L^*_{ac}}-1)}$$

After rearranging the last equivalence which has been presented above the following form obtained:

$$\frac{\sqrt{U_d}}{wB_{rmax}} \cong \sqrt{\frac{\nu_{iz}}{\nu_e}}\sqrt{\frac{e}{M}}\frac{1}{K_W(e^{\langle\alpha\rangle L^*_{ac}}-1)}. \tag{42}$$

This is a relation consists of discharge voltage, maximum magnetic field, and acceleration channel width with the other terms which mentioned in this section previously.

D. Wall Erosion Criterion for the Life Time

Wall erosion is the most important parameter which could limit the life time of the thruster. Indeed the source of this erosion is the collisions between ions and the wall in the acceleration layer. Determining the value of the erosion in the specific operational time is one of the important parameter which should be investigated to design a thruster. Fig. 9 shows the erosion of the wall in the acceleration channel where the maximum erosion occurs during the operation of the thruster. The angle φ is the rotation angle of the flow during passing the rubbed region. This angle is usually about 15 to 20 degree. The term $\delta(t_{rotation})$ is the erosion thickness of the wall during the flow rotates

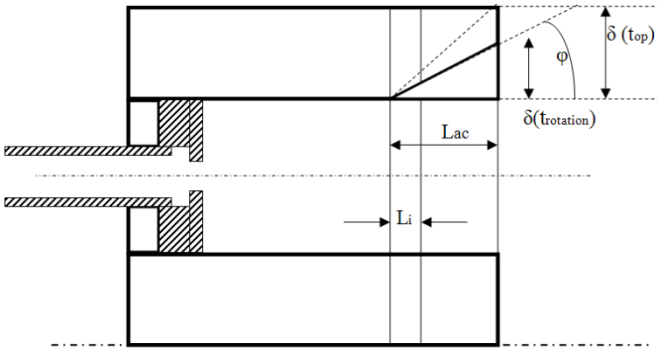

Figure 9. A schematic view of wall erosion with the required dimensions.

with the angle φ. The term $\delta(t_{op})$ is the potential erosion thickness specified for the whole operational time of the thruster. The rotation time of the flow with the angle φ could be calculated by using Eq. (43): [9]

$$t_{rotation} = \frac{\delta_W}{\frac{I_{iW}}{2\pi d L_{ac}} S_v}. \tag{43}$$

In this relation δ_W, I_{iW}, and S_v are wall thickness, the ion current to the wall, and volume sputtering coefficient of the ceramic (see Fig. 10) which is the material of the wall respectively.

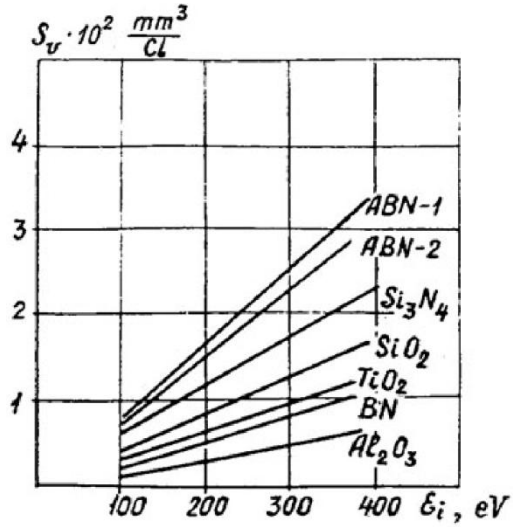

Figure 10. Volume sputtering coefficient for different ceramics versus ion energy from Ref. 9.

The ion current could be calculated with the relation:

$$\Delta U_{aci} = \frac{(P_{jet}/\gamma)}{I_{\dot{m}} - I_{iW}}. \tag{44}$$

Where ΔU_{aci}, P_{jet}, and γ are acceleration potential of ion in acceleration layer, jet power, and total thrust correction coefficient which is the product of both the plume divergence correction coefficient and multiply charged species correction coefficient. The value of γ is about 0.9.

It is possible to determine the erosion thickness of the wall during the ions collisions with the following relation:

$$\delta(t_{op}) = C_t ln\left(1 + \frac{t_{op}}{t_{rotation}}\right). \tag{45}$$

Where C_t, t_{op} are a constant, and given operation time respectively. The thickness $\delta(t_{op})$ must satisfy $\delta(t_{op}) \leq \delta_W$.

III. Preliminary Design of a Hall Thruster

In this section we proceed by specifying the operation input values for a typical Hall thruster. Then every part which has been mentioned in section II will be applied to achieve the required dimensions, operational values, and preliminary values for designing the magnetic circuit.

A. General Dimensions and Operational Values

The operation values for the thruster are:

- Thrust: 80 mN
- Discharge Voltage: 300 Volts
- Specific Impulse: 1600 sec
- Propellant: Xenon
- Operational Time: 290 days

At first acceleration voltage of the ions, Xenon atom temperature, and electron temperature must be calculated. Then, by using Eq. (22) it is possible to obtain the mean diameter value. Regarding to the previous explanation the temperature of Xenon atoms varies 800 to 1000K for the discharge voltage interval 150 to 350 volts. Then, for 300 volts the atom temperature is:

$$\frac{T_a - 800}{1000 - 800} = \frac{U_d - 150}{350 - 150} \xrightarrow{U_d=300} T_a = 950K\,. \tag{46}$$

Also as described in previous explanation the temperature of electrons varies 10 to 20eV for the discharge voltage interval 150 to 900 volts. Then, for 300 volts the electron temperature is:

$$T_{eV} = \frac{U_d - 150}{75} + 10 \xrightarrow{U_d=300} T_{eV} = 12eV\,. \tag{47}$$

By Using Eq. (19) and the electron temperature the ionization reaction rate coefficient has the following value:

$$\begin{gathered}\langle \sigma_i V_e \rangle \cong \langle \sigma_i \rangle \bar{V}_e = 10^{-20}\left[-(1.031 \times 10^{-4})T_{eV}^2 + 6.386e^{-12.127/T_{eV}}\right]\left(\frac{8eT_{eV}}{\pi m}\right)^{1/2}, T_{eV} > 5eV \\ \xrightarrow{T_{eV}=12} \langle \sigma_i V_e \rangle = 5.4 \times 10^{-14}\left(\frac{m^3}{s}\right).\end{gathered} \tag{48}$$

The electrical potential in the ionization layer is about 2.5 to 3 times the first Xenon ionization potential. Also the cathode electrical potential is about 10 to 20 volts. [10] Then, the discharge voltage could be written in the following form: [6]

$$U_d = \Delta U_{aci} + \big((2.5, \dots, 3) + 1\big)\varphi_i + U_c\,. \tag{49}$$

In Eq. (49) U_c is the cathode potential which chosen 20 volts. The first ionization potential is 12.1eV. The number one in the parenthesis is related to the anode potential. By choosing $3\varphi_i$ as potential in the ionization layer the acceleration potential of ion in acceleration layer has the value:

$$\Delta U_{aci} = 300 - (3 + 1)12.1 - 20 = 231.6\ volts\,. \tag{50}$$

The values of the ion and atom velocity are:

$$V_i = \sqrt{\frac{2eU_d}{M}} = \sqrt{\frac{2 \times 1.6 \times 10^{-19} \times 300}{2.18 \times 10^{-25}}} = 20984.92\ \left(\frac{m}{s}\right), \tag{51}$$

$$V_a = \sqrt{\frac{8K_B T_a}{\pi M}} = \sqrt{\frac{8 \times 1.38 \times 10^{-23} \times 950}{\pi \times 2.18 \times 10^{-25}}} = 391.33 \left(\frac{m}{s}\right).$$

By using Eq. (22) the channel mean diameter has the value:

$$\frac{\dot{m}_a}{d} \geq \xi \frac{\pi M V_i V_a}{\langle \sigma_i V_e \rangle} = 0.5 \times \frac{\pi \times 2.18 \times 10^{-25} \times 20984.92 \times 391.33}{5.4 \times 10^{-14}} \cong 5.2 \times 10^{-5} \left(\frac{kg}{s.m}\right). \quad (52)$$

To calculate the mass flow rate through the anode, the total propellant mass flow rate must be calculated using thrust F definition. In the following equation V_{ex}, I_{sp}, and g are propellant exit velocity, specific impulse, and gravity constant respectively.

$$F = \dot{m} V_{ex} = \dot{m}(I_{sp} g) \Longrightarrow 0.08 = \dot{m} \times (1600 \times 9.81) \Longrightarrow \dot{m} = 5.1 \times 10^{-6} \left(\frac{kg}{s}\right). \quad (53)$$

By reviewing the experimental data the cathode mass flow rate is typically 5% to 10% of the anode mass flow rate. Now by choosing the criterion 10% it is possible to determine the anode mass flow rate as below: [10]

$$\dot{m} = \dot{m}_a + \dot{m}_c = \dot{m}_a + 0.1\dot{m}_a = 1.1\dot{m}_a \Longrightarrow \dot{m}_a = 4.6 \times 10^{-6} \left(\frac{kg}{s}\right). \quad (54)$$

Then, the channel mean diameter has the value:

$$d \leq 0.088\text{m} \Longrightarrow \text{d}_{\max} = 0.088 \text{ m} = 88 \text{ mm}. \quad (55)$$

By using the dimension criterion which has been presented in Ref. 9 the general dimensions have the following values:

$$w \leq 0.25\text{d}, L = (1, \dots, 2)w, \delta_W \approx 0.1d, d_{th} \approx 2d, L_{th} \approx d. \quad (56)$$

Where d_{th}, and L_{th} are thruster diameter and length as shown in Fig. 4.

$$\begin{gathered} w = 0.25\text{d} = 0.022\, m = 22\, mm \\ \delta_W = 0.1d \approx 0.009\, m = 9\, mm \\ L = w + 2\delta_W \approx 0.04\, m = 40\, mm \\ d_{th} = 2d = 0.176\, m = 176\, mm \\ L_{th} = d = 0.088\, m = 88\, mm \\ d_{inc} = d - w = 0.066\, m = 66\, mm \\ d_{in} = d - w - 2\delta_W = 0.048\, m = 48\, mm \\ d_{ouc} = d + w = 0.11\, m = 110\, mm \\ d_{ou} = d + w + 2\delta_W = 0.128\, m = 128\, mm \end{gathered} \quad (57)$$

To determine the ion current to the wall it is necessary to calculate the jet power and the acceleration power as below: [10]

$$P_{jet} = \frac{F^2}{2\dot{m}_a}\eta_c\,, \qquad P_{ac} = \frac{P_{jet}}{\gamma}\,. \tag{58}$$

Where $\eta_c = \frac{\dot{m}_a}{\dot{m}} = \frac{1}{1+\frac{\dot{m}_c}{\dot{m}_a}} = \frac{1}{1+K_c}$ is the cathode efficiency.

$$P_{jet} = \frac{F^2}{2\dot{m}_a}\eta_c = \frac{(0.08)^2}{2\times 4.6\times 10^{-6}}\frac{1}{1.1} = 633\ Watt \qquad P_{ac} = \frac{P_{jet}}{\gamma} = \frac{633}{0.9} = 703.3\ Watt \tag{59}$$

The current related to the anode mass flow rate has the following value:

$$I_{\dot{m}} = \frac{e\dot{m}_a}{M} = 3.4\ A\,. \tag{60}$$

By using Eq. (44) the ion current to the wall calculated as below:

$$\Delta U_{aci} = \frac{(P_{jet}/\gamma)}{I_{\dot{m}} - I_{iW}} \Longrightarrow I_{iW} = 0.36\ A\,. \tag{61}$$

For calculating the acceleration layer length there is empirical relations which has the following forms:

$$I_{iW} = 0.5\mathrm{K_{iW}}\, I_{\dot{m}}\,, \qquad \mathrm{K_{iW}} = 1.5\frac{\mathrm{L_{ac}}}{\mathrm{d}}\,. \tag{62}$$

By using above relations:

$$\mathrm{K_{iW}} = 0.21\,, \qquad \mathrm{L_{ac}} = 0.0123\ \mathrm{m} = 12.3\ \mathrm{mm}\,. \tag{63}$$

In Ref. 9 described that the ionization layer begins at the length of the channel where the magnetic field is at 0.6 of its maximum value or $B_r \geq 0.6B_{rmax}$. To obtain a profile for the variation of the magnetic field along the channel length the following calculation has done.

$$\int_{B_{rmax}}^{B_r} \frac{dB_r}{B_r} = -\frac{1}{L}\int_0^z K_1\,dz \Longrightarrow ln\left(\frac{B_r}{B_{rmax}}\right) = -\frac{1}{L}K_1 z + K_2 \tag{64}$$

In Eq. (64) the origin of the axis as shown in Fig. 11 is at the exit of the thruster.

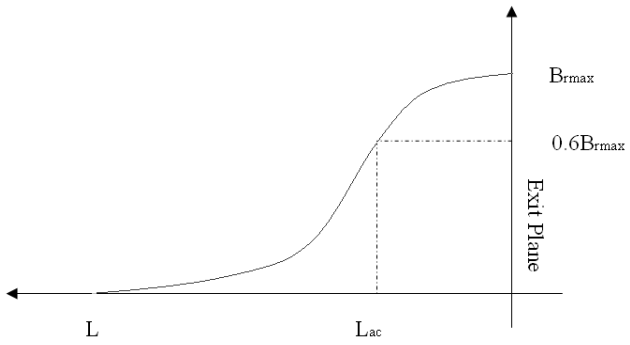

Figure 11. Distribution of the magnetic field along the channel.

To specify the boundary condition it is required to investigate that typical value of the magnetic field at the region near the anode. By reviewing the literatures the percentage of the magnetic field in this region is about 0.22 of the maximum value of the magnetic field. Then the following boundary condition applied to solve the Eq. (64).

$$\begin{gathered} z = 0 \Longrightarrow B_r = B_{rmax} \Longrightarrow K_2 = 0 \\ z = L \Longrightarrow B_r = 0.22B_{rmax} \Longrightarrow K_1 \cong 1.5 \\ ln\left(\frac{B_r}{B_{rmax}}\right) = -\frac{1.5}{L}z \Longrightarrow B_r = B_{rmax}\, e^{-\frac{1.5z}{L}} \end{gathered} \tag{65}$$

The last relation in Eq. (65) gives the magnetic field in every point along the channel length and at the mean radius of the channel. Putting L_{ac} value in this relation gives following criterion for the magnetic field:

$$B_r = B_{rmax}\, e^{-\frac{1.5z}{L}} = B_{rmax}\, e^{-\frac{1.5\times 0.0123}{0.04}} = 0.63B_{rmax} \tag{66}$$

In this thruster with the mentioned input data the ionization will begin when the magnetic field is at 63% of its maximum value. As described earlier the discharge current is 1.2 to 1.4 of $I_{\dot{m}}$. Then the discharge current is:

$$I_d = (1.2, \ldots, 1.4)I_{\dot{m}} \approx 1.4(3.4) = 4.76\ A\,. \tag{67}$$

The discharge input power and the number of ions and electrons with quasi-neutrality assumption are as below:

$$\begin{gathered} P_{\,ind} = \mathrm{I_d U_d} = 4.76 \times 300 = 1428\mathrm{Watt}\,, \\ S_{ch} = \pi dw = \pi(0.088)(0.022) = 6.1 \times 10^{-3} m^2\,, \\ n_e \cong n_i \cong \frac{\dot{m}_a}{MV_iS_{ch}} = \frac{\dot{m}_a}{M\sqrt{\frac{2e(3\varphi_i)}{M}}S_{ch}} = 4.7 \times 10^{17}\left(\frac{par}{m^3}\right). \end{gathered} \tag{68}$$

Also the length of the ionization layer could be calculated with below equation. [8]

$$L_i = 3\lambda_i \approx 3\frac{\sqrt{K_B T_a e\varphi_i}}{\dot{m}_a\langle\sigma_i V_e\rangle}S_{ch} = 0.0117m = 11.7\ mm \tag{69}$$

After the previous calculations it is the time to find the magnetic field value by using Eq. (42). In this equation the term $\sqrt{\frac{\nu_e}{\nu_{iz}}}$ estimated from Fig. 5 with the energy $\sqrt{\varepsilon_e} = \sqrt{12} = 3.46\ (eV)^{\frac{1}{2}}$ the related value for $\sqrt{\frac{\nu_e}{\nu_{iz}}}$ is about 5.1. By Using Eqs. (40) and (41) the coefficient K_W has the following value:

$$\frac{\Delta V_W}{V_o} = 1 - \cos 2\alpha_s \xrightarrow{\alpha_s = 23^o} \frac{\Delta V_W}{V_o} = 1 - \cos 2(23) = 0.3\ ,$$
$$K_W = \underbrace{\frac{(n_e V_e)_W}{(n_e V_e)_o}}_{0.1} \frac{\Delta V_W}{V_o} = (0.1)(0.3) = 0.03\ . \tag{70}$$

In addition by using Eq. (35) the term $\langle\alpha\rangle L_{ac}^*$ is:

$$\frac{j_d}{j_{\dot{m}}} = \frac{exp(\langle\alpha\rangle L_{ac}^*)}{exp(\langle\alpha\rangle L_{ac}^*) - 1} = 1.4 \Longrightarrow \langle\alpha\rangle L_{ac}^* = 1.25\ . \tag{71}$$

Putting the required value in Eq. (42) gives following value for B_{rmax} .

$$\frac{\sqrt{U_d}}{wB_{rmax}} \cong \sqrt{\frac{\nu_{iz}}{\nu_e}} \sqrt{\frac{e}{M}} \frac{1}{K_W(e^{\langle\alpha\rangle L_{ac}^*} - 1)} \Longrightarrow B_{rmax} = 0.014\ Tesla = 14\ mTesla \tag{72}$$

Now we check the Eq. (1) for electron and ion Larmor radius.

$$E_z \cong \frac{\Delta U_{aci}}{L_{ac}} = 1.93 \times 10^4 \left(\frac{volts}{m}\right)$$
$$r_{Le} = \frac{mE_z}{eB_{rmax}^2} = 0.00043m \ll (w = 0.022\ m) \tag{73}$$
$$r_{Li} = \frac{ME_z}{eB_{rmax}^2} = 102.7m \gg (w = 0.022\ m)$$

It is possible to find thruster efficiency with the relation which has mentioned below.

The most important criterion, thruster lifetime, must be checked here. The erosion thickness should be lower than the wall thickness to prevent the magnetic circuit form the probable damage. To calculate the rotation time the volume sputtering coefficient is required. For boron nitride (ABN) and for ion energy $\varepsilon_i = \frac{\frac{1}{2}MV_{ex}^2}{e} \cong 168\ eV$ the S_v is $1.5 \times 10^{-11} \left(\frac{m^3}{C}\right)$. By using Eq. (43) the rotation time is:

$$t_{rotation} = \frac{\delta_W}{\frac{I_{iW}}{2\pi d L_{ac}} S_v} = 1.25 \times 10^7\ s\ . \tag{74}$$

This erosion occurred in the acceleration layer. With the φ angle equal to 17 degree the erosion thickness is:

$$\delta_{(t_{rotation})} = L_{ac}\, tg(17^o) \cong 0.004\ m\ . \tag{75}$$

By using Eq. (45) and set $t = t_{rotation}$ the coefficient C_t has the value:

$$0.004 = C_t ln\left(1 + \frac{t_{rotation}}{t_{rotation}}\right) \Rightarrow C_t = 0.006\,. \tag{76}$$

Now by converging the operational time from day to second it has the value $2.5 \times 10^7\ s$. Then the erosion thickness for the given 290 days is:

$$\delta_{(t_{op})} = (0.006) ln\left(1 + \frac{2.5 \times 10^7}{1.25 \times 10^7}\right) \Rightarrow \delta_{(t_{op})} = 0.0066\ m < (\delta_W = 0.009\ m)\,. \tag{77}$$

The erosion thickness is lower than the wall thickness then we proceed to calculate the magnetic circuit parameters. Figs. 12 and 13 show the magnetic circuit and its electrical circuit respectively. In Fig. 12, the red lines are the magnetic flux direction in each part. For the outer and inner electromagnet these lines show the direction of the electromotive forces (ε_o, ε_i) too.

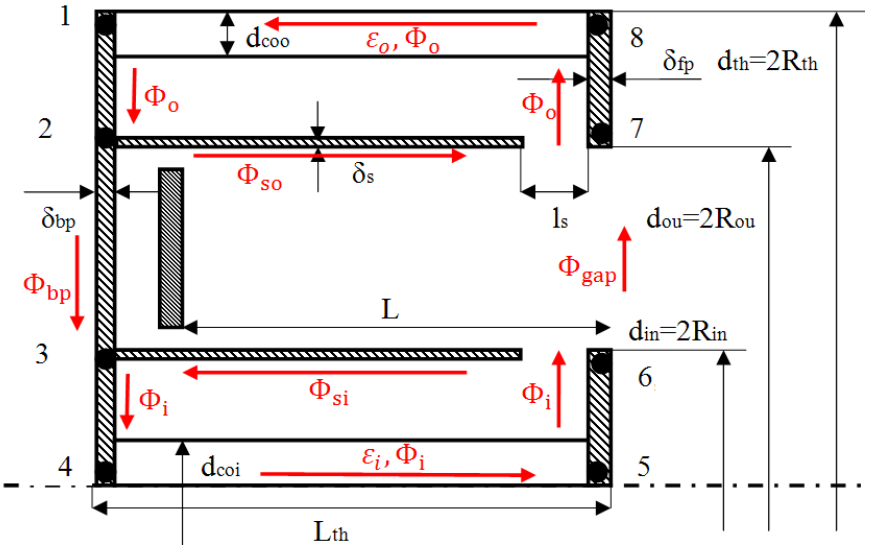

Figure 12. Schematic of the magnetic circuit, its parts and dimensions.

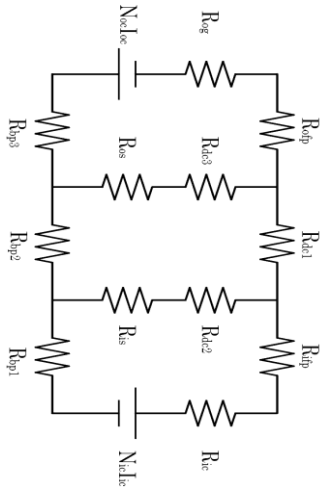

Figure 13. Electrical circuit equivalent to magnetic circuit from Ref. 10.

In Fig. 13, the source $N_{oc}I_{oc}$ is electromotive force ε_o of the outer electromagnet (E.M.). In addition the source $N_{oi}I_{oi}$ is the electromotive force ε_i of outer electromagnet. The term N is the number of the wire turns of the coil for the electromagnet. Also in Fig. 12, magnetic fluxes ($\Phi = BA$) passing through sources are Φ_o for outer electromagnet and Φ_i for inner electromagnet. Usually the inner wire turns number is 1.6 times the outer wire turns number. [8,9] In this thruster one electromagnet is at the center of the thruster and four outer are in each quarter with symmetrical form as shown in Fig. 14.

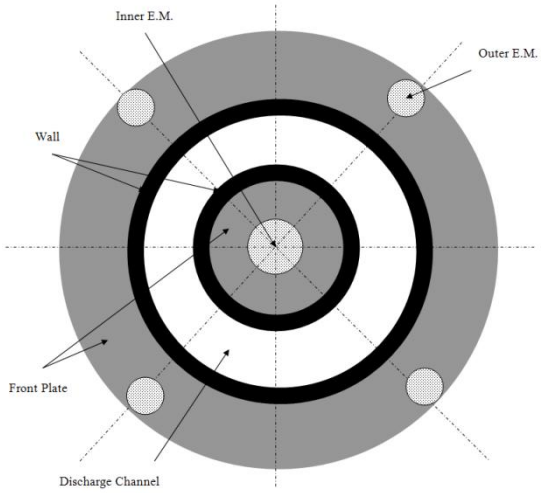

Figure 14. Front view of the electromagnet arrangement.

By using Fig. 12, it is possible to specify every resistor in Fig. 13. For this circuit there are three loops which specified below.

Loop1:

This loop consists of five resistors. Resistor R_{ic} is between points 4, 5 or is the inner electromagnet resistance. Resistor $R_{bp\,1}$ is between points 3, 4. R_{is} is inner screen Resistance. $R_{gap\,,is}$ is the resistor between the inner screen and point 6. And also R_{ifp} is between points 5, 6.

Loop2:

This loop consists of five resistors. Resistor R_{oc} is between points 1, 8 or is the outer electromagnet resistance. Resistor $R_{bp\,3}$ is between points 1, 2. R_{os} is outer screen Resistance. $R_{gap\,,os}$ is the resistor between the outer screen and point 7. And also R_{ofp} is between points 7, 8.

Loop3:

This loop consists of $R_{gap\,67}$ between points 6, 7; $R_{bp\,2}$ between points 2, 3; and R_{is}, $R_{gap\,,is}$, R_{os}, $R_{gap\,,os}$.

By using Kirchhoff's law it is possible to make a relation between electromotive force, magnetic resistance, and magnetic flux. Kirchhoff's law is a simplification of Faraday's law of induction for the special case where there is no fluctuating magnetic field linking the closed loop. Therefore, it practically suffices for explaining circuits containing only resistors and capacitors. Now we proceed to introduce some resistors.

$$\begin{gathered} R_1 = R_{bp\,1} + R_{ic} + R_{ifp} \\ R_2 = R_{bp\,3} + R_{oc} + R_{ofp} \\ R_3 = R_{gap\,67} \\ R_4 = R_{is} + R_{gap\,,is} \\ R_5 = R_{os} + R_{gap\,,os} \\ R_6 = R_{bp\,2} \end{gathered} \tag{78}$$

The summation of the magnetic flux at points 6, and 7 are:

$$\begin{gathered} \begin{cases} Point\ 6\colon \Phi_i - \Phi_{gap} - \Phi_{si} = 0 \\ Point\ 7\colon \Phi_{so} + \Phi_{gap} - \Phi_o = 0 \end{cases} \Longrightarrow \begin{cases} R_1\Phi_i - R_1\Phi_{si} = R_1\Phi_{gap} \\ R_2\Phi_o - R_2\Phi_{so} = R_2\Phi_{gap} \end{cases}, \\ \xrightarrow{Point\ 6+Point\ 7} R_1\Phi_i + R_2\Phi_o - (R_1\Phi_{si} + R_2\Phi_{so}) = (R_1 + R_2)\Phi_{gap} \ . \end{gathered} \tag{79}$$

The summation of the magnetic flux at points 2, and 7 are:

$$\begin{cases} Point\ 2\colon \Phi_o - \Phi_{so} - \Phi_{bp} = 0 \\ Point\ 7\colon \Phi_{so} + \Phi_{gap} - \Phi_o = 0 \end{cases} \xrightarrow{Point\ 2+Point\ 7} \Phi_{gap} = \Phi_{bp} \ . \tag{80}$$

The Kirchhoff's law for loop3 has the following form:

$$\Phi_{so}R_5 - \Phi_{gap}R_3 + \Phi_{si}R_4 - \Phi_{gap}R_6 = 0 \longrightarrow \Phi_{so}R_5 + \Phi_{si}R_4 = \Phi_{gap}(R_3 + R_6)\,. \tag{81}$$

The Kirchhoff's law for loop1 and 2 have the following forms:

$$\begin{gathered} \begin{cases} Loop\ 1\colon \varepsilon_1 - \Phi_i R_1 - \Phi_{si}R_4 = 0 \\ Loop\ 2\colon \varepsilon_2 - \Phi_o R_2 - \Phi_{so}R_5 = 0 \end{cases} \xrightarrow{Loop\ 1+Loop\ 2} \varepsilon_1 + \varepsilon_2 - (\Phi_i R_1 + \Phi_o R_2) = \Phi_{si}R_4 + \Phi_{so}R_5\,, \\ \xrightarrow[Eq.(81)]{} \varepsilon_1 + \varepsilon_2 - (\Phi_i R_1 + \Phi_o R_2) = \Phi_{gap}(R_3 + R_6)\,. \end{gathered} \tag{82}$$

The summation of Eq. (79) and Eq. (82) is:

$$(\varepsilon_1 + \varepsilon_2) - (\Phi_{si} R_1 + \Phi_{so} R_2) = \Phi_{gap} (R_1 + R_2 + R_3 + R_6) . \tag{83}$$

For points 2 and 6 there are $\Phi_o = \Phi_{so} + \Phi_{gap}$, and $\Phi_i = \Phi_{gap} + \Phi_{si}$ respectively. By putting these relations in loop1 and loop2 relations the result is as below:

$$\begin{cases} Loop\ 1: \varepsilon_1 - \Phi_i R_1 - \Phi_{si} R_4 = 0 \\ Loop\ 2: \varepsilon_2 - \Phi_o R_2 - \Phi_{so} R_5 = 0 \end{cases} \longrightarrow \begin{cases} Loop\ 1: \varepsilon_1 - \left(\Phi_{gap} + \Phi_{si}\right) R_1 - \Phi_{si} R_4 = 0 \\ Loop\ 2: \varepsilon_2 - \left(\Phi_{gap} + \Phi_{so}\right) R_2 - \Phi_{so} R_5 = 0 \end{cases}$$
$$\longrightarrow \begin{cases} \Phi_{si} = \dfrac{\varepsilon_1 - \Phi_{gap} R_1}{(R_1 + R_4)} \\ \Phi_{so} = \dfrac{\varepsilon_2 - \Phi_{gap} R_2}{(R_2 + R_5)} \end{cases} . \tag{84}$$

By putting Eq. (84) in Eq. (81) the following relation has been obtained.

$$\left[\frac{\varepsilon_2 - \Phi_{gap} R_2}{(R_2 + R_5)}\right] R_5 + \left[\frac{\varepsilon_1 - \Phi_{gap} R_1}{(R_1 + R_4)}\right] R_4 = \Phi_{gap} (R_3 + R_6)$$
$$\longrightarrow \frac{\varepsilon_2}{(R_2 + R_5)} R_5 + \frac{\varepsilon_1}{(R_1 + R_4)} R_4 = \Phi_{gap} \left(\frac{R_2 R_5}{(R_2 + R_5)} + \frac{R_1 R_4}{(R_1 + R_4)} + R_3 + R_6\right) . \tag{85}$$

In Eq. (85) every resistor is obvious and because the current passing through the sources are discharge current then $\varepsilon_i = 1.6\varepsilon_o$. The magnetic flux Φ_{gap} could be calculated with integration in the channel. Then the only unknown parameter in Eq. (85) is one of the electromotive forces. Because the geometry is symmetrical only one quarter of the channel will be considered for calculation of magnetic flux Φ_{gap} as below.

$$B_r = B_{rmax}\, e^{-\frac{1.5z}{L}}, A = \pi d L, dA = (\pi d) dz ;$$
$$\Phi_{gap} = B_r A = \left(\frac{1}{4}\right)\left(2 \int_0^L B_{rmax}\, e^{-\frac{1.5z}{L}} (\pi d) dz\right) = \frac{1}{2} \int_0^L B_{rmax}\, e^{-\frac{1.5z}{L}} (\pi d) dz \tag{86}$$
$$= \frac{\pi d B_{rmax}}{2} \left(-\frac{L}{2}\right) e^{-\frac{1.5z}{L}} \Big|_0^L = \frac{\pi d B_{rmax} L}{4} \left[1 - \frac{1}{e^{1.5}}\right] = 3.01 \times 10^{-5}\ (Wb) .$$

The magnetic resistance is defined as $R_j = \frac{L_j}{\mu_j A_j}$. Where L_j, A_j, μ_j are the length of the element, cross section of the element where the flux passing through it, and the magnetic permeability of the element respectively. The unit of this resistance is $\frac{1}{H}$. The magnetic permeability for vacuum is $\mu_0 = 4\pi \times 10^{-7}\ \left(\frac{H}{m}\right)$. For the nickel alloys the magnetic permeability is $(\mu_r = 100, \ldots, 600)$ times the vacuum permeability. The chosen magnetic permeability is 600. To calculate the magnetic resistance some parameters are introduced here as below:

$$\begin{cases} d_{coi} \approx 0.66 B_{rmax} = 1.2 \times 10^{-5} \dfrac{\sqrt{U_d}}{w} = 0.0092\ m \\ d_{coo} \approx 0.44 B_{rmax} = 0.8 \times 10^{-5} \dfrac{\sqrt{U_d}}{w} = 0.0062\ m \\ \delta_{bp} \approx 0.1 B_{rmax} = 0.18 \times 10^{-5} \dfrac{\sqrt{U_d}}{w} = 0.0014\ m \\ For: d = 70, \ldots, 290\ mm \Longrightarrow \begin{cases} \delta_s \approx 1\ mm \\ l_s \approx 5\ mm \\ \delta_{fp} \approx 2, .., 3\ mm \xrightarrow{choose} 3\ mm \end{cases} \end{cases} . \tag{87}$$

These parameters are for optimum operation of a stationary plasma thruster. All of the magnetic resistors and their formulas are arranged as the following:

1) R_1 consists of three resistors as below:

$$R_{ic} = \frac{L_{th}}{\mu_r \mu_0 \frac{1}{4}\left(\pi \frac{d_{coi}^2}{4}\right)} \Rightarrow R_{ic} = 7.02\times10^6\left(\frac{1}{H}\right),$$

$$R_{bp1} = \frac{R_{in} - \frac{d_{coi}}{2}}{\mu_r \mu_0 \delta_{bp} \frac{1}{4}\left(\pi \frac{d_{in} + d_{coi}}{2}\right)} \Rightarrow R_{bp1} = 0.82\times10^6\left(\frac{1}{H}\right),$$

$$R_{ifp} = \frac{R_{in} - \frac{d_{coi}}{2}}{\mu_r \mu_0 \delta_{fp} \frac{1}{4}\left(\pi \frac{d_{in} + d_{coi}}{2}\right)} \Rightarrow R_{ifp} = 0.38\times10^6\left(\frac{1}{H}\right).$$

2) R_2 consists of three resistors as below:

$$R_{oc} = \frac{L_{th}}{\mu_r \mu_0 \left(\pi \frac{d_{coo}^2}{4}\right)} \Rightarrow R_{oc} = 3.86\times10^6\left(\frac{1}{H}\right),$$

$$R_{bp3} = \frac{R_{th} - R_{ou} - d_{coo}}{\mu_r \mu_0 \delta_{bp} \frac{1}{4}\left(\pi \frac{d_{th} - 2d_{coo} + d_{ou}}{2}\right)} \Rightarrow R_{bp3} = 1.47\times10^5\left(\frac{1}{H}\right),$$

$$R_{ofp} = \frac{R_{th} - R_{ou} - d_{coo}}{\mu_r \mu_0 \delta_{fp} \frac{1}{4}\left(\pi \frac{d_{th} - 2d_{coo} + d_{ou}}{2}\right)} \Rightarrow R_{ofp} = 0.69\times10^5\left(\frac{1}{H}\right).$$

3) Calculation of μ_{plasma} and determination of R_3 :

$$\sigma_{en}(T_e) = 6.6\times10^{-19}\left[\frac{\frac{T_{eV}}{4}-0.1}{1+\left(\frac{T_{eV}}{4}\right)^{1.6}}\right] \xrightarrow{T_{eV}=12eV} \sigma_{en}(T_e) = 2.8\times10^{-19}\left(m^2\right)$$

$$V_a = \sqrt{\frac{\gamma K_B T_a}{M}} = \sqrt{\frac{1.666\times1.38\times10^{-23}\times950}{2.18\times10^{-25}}} = 316.5\left(\frac{m}{s}\right)$$

$$\dot{m}_a = V_a n_a M S_{ch} \rightarrow n_a = \frac{5.1\times10^{-6}}{245.2\times2.18\times10^{-25}\times6.1\times10^{-3}} = 1.21\times10^{19}\left(\frac{Par}{m^3}\right)$$

$$\nu_{en} = \sigma_{en}(T_e) n_a \sqrt{\frac{8K_B T_e}{\pi(m)}} = 2.8\times10^{-19}\times1.21\times10^{19}\times21526.8 = 1798329.6\left(\frac{1}{s}\right)$$

$$\nu_{en,anom} = \alpha_B \omega_c = \frac{1}{16}\frac{|q|B}{m} = \frac{1}{16}\frac{1.6\times10^{-19}\times0.014}{9.1\times10^{-31}} = 153846153.8\left(\frac{1}{s}\right)$$

$$\ln\Lambda = 23 - \frac{1}{2}\ln\left(\frac{10^{-6} n_e}{T_{eV}^3}\right) \rightarrow \ln\Lambda = 13.3$$

$$\nu_{ei} = 2.9\times10^{-12}\frac{n_e \ln\Lambda}{T_{eV}^{3/2}} \rightarrow \nu_{ei} = 436089.5\left(\frac{1}{s}\right)$$

$$\nu_{ee} = 5\times10^{-12}\frac{n_e \ln\Lambda}{T_{eV}^{3/2}} \rightarrow \nu_{ee} = 751878.4\left(\frac{1}{s}\right)$$

$$\nu_e = \nu_{en} + \nu_{en,anom} + \nu_{ei} + \nu_{ee}$$

$$\mu_p = \frac{|q|}{m\nu_e} = \frac{1.6\times10^{-19}}{9.1\times10^{-31}\times(1798329.6 + 153846153.8 + 436089.5 + 751878.4)} = 1121.1\left(\frac{C.s}{kg}\right)$$

$$\mu_{plasma} = \frac{1}{\mu_p}\left(\frac{L}{I_d}\right) = \frac{1}{1121.1}\left(\frac{0.04}{4.76}\right) = 7.5\times10^{-6}\left(\frac{H}{m}\right) \rightarrow \mu_{r,plasma} = \frac{7.5\times10^{-6}}{4\pi\times10^{-7}} \cong 6$$

$$R_{gap67} = \frac{w + 2\delta_W}{\mu_{r,plasma}\mu_0 \frac{1}{4}(\pi L d)} = \frac{1}{6\times4\pi\times10^{-7}\times0.25\times\pi\times0.088} = 1.92\times10^6\left(\frac{1}{H}\right)$$

$$\Rightarrow R_{gap67} = 1.92\times10^6\left(\frac{1}{H}\right)$$

The equations for the electron frequencies obtained from Ref. 3. For this calculation assumed that the Xenon atoms enters the channel with acoustic velocities ($V_a = \sqrt{\frac{\gamma K_B T_a}{M}}$). Also $\nu_{en,anom}$ is the anomalous frequency which is due to the interaction between the electromagnetic wave and the electrons.

4) R_4 consists of two resistors as below:

$$R_{is} = \frac{L_{th} - l_s}{\mu_r \mu_0 \delta_s \frac{\pi}{4} d_{in}} \Rightarrow R_{is} = 2.92\times10^6\left(\frac{1}{H}\right),$$

$$R_{gap,is} = \frac{l_s}{\mu_r \mu_0 l_s \frac{\pi}{4} d_{in}} \Rightarrow R_{gap,is} = 21.1\times10^6\left(\frac{1}{H}\right).$$

5) R_5 consists of two resistors as below:

$$R_{os} = \frac{L_{th} - l_s}{\mu_r \mu_0 \delta_s \frac{\pi}{4} d_{ou}} \Rightarrow R_{os} = 1.1\times10^6\left(\frac{1}{H}\right),$$

$$R_{gap,os} = \frac{l_s}{\mu_r \mu_0 l_s \frac{\pi}{4} d_{ou}} \Rightarrow R_{gap,os} = 7.92\times10^6\left(\frac{1}{H}\right).$$

6) R_6 consists of one resistors as below:

$$R_{bp2} = \frac{R_{ou} - R_{in}}{\mu_r \mu_0 \delta_{bp} \frac{\pi}{4} d} \Rightarrow R_{bp2} = 5.5\times10^5\left(\frac{1}{H}\right).$$

Then the values of resistors one to six are:

$$R_1 = 8.22\times10^6\left(\frac{1}{H}\right), R_2 = 4.1\times10^6\left(\frac{1}{H}\right), R_3 = 1.92\times10^6\left(\frac{1}{H}\right)$$
$$, R_4 = 24.02\times10^6\left(\frac{1}{H}\right), R_5 = 9.02\times10^6\left(\frac{1}{H}\right), R_6 = 5.5\times10^5\left(\frac{1}{H}\right).$$

By using Eq. (85) and the obtained values for resistors and magnetic fluxes the value of ε_2, N_1, N_2 are:

$$\varepsilon_2 = 182.08\ (A) \longrightarrow \mathrm{N}_2 = 38 \longrightarrow \mathrm{N}_1 = 61\ .$$

The power consumption of the magnetic system is 0.5% to 4% of the discharge power. The chosen value 0.5% for this thruster. Then the electrical resistance for the magnetic system obtained as the following:

$$P_{mag} = 0.05P_{ind} = 7.14\,Watt \longrightarrow P_{mag} = I_d^2 R_m \xrightarrow{R_m \text{ is electrical resistance .}} R_m = 0.32\Omega$$

The electrical resistance could be shown as $R_m = \frac{\rho L_m}{S_m}$. In this relation ρ, L_m, S_m are specific resistance of the wire, length of the wire, and cross section of the wire respectively. The selected material for the wire is copper with

operational temperature as 600 K and the initial temperature of the system is 20^{oc}. [11] The specific resistance of the copper is $0.0172 \times 10^{-6}\ \Omega.m$. Then the required length of the wire and its diameter are:

$$L_m = N_1 d_{coi}\pi + 4N_2 d_{coo}\pi = 4.72\ m$$
$$\rho_{600} = \rho[1 + \alpha(T_2 - T_1)] = 0.0383 \times 10^{-6}\Omega.m$$
$$\longrightarrow S_m = 0.62 \times 10^{-6}\ m^2$$
$$\longrightarrow d_m = 0.84 \times 10^{-3}\ m$$

The total length of the wire for the magnetic system is 4.72 m with 0.84×10^{-3}m diameter. Fig. 15 shows the schematic view of the designed thruster.

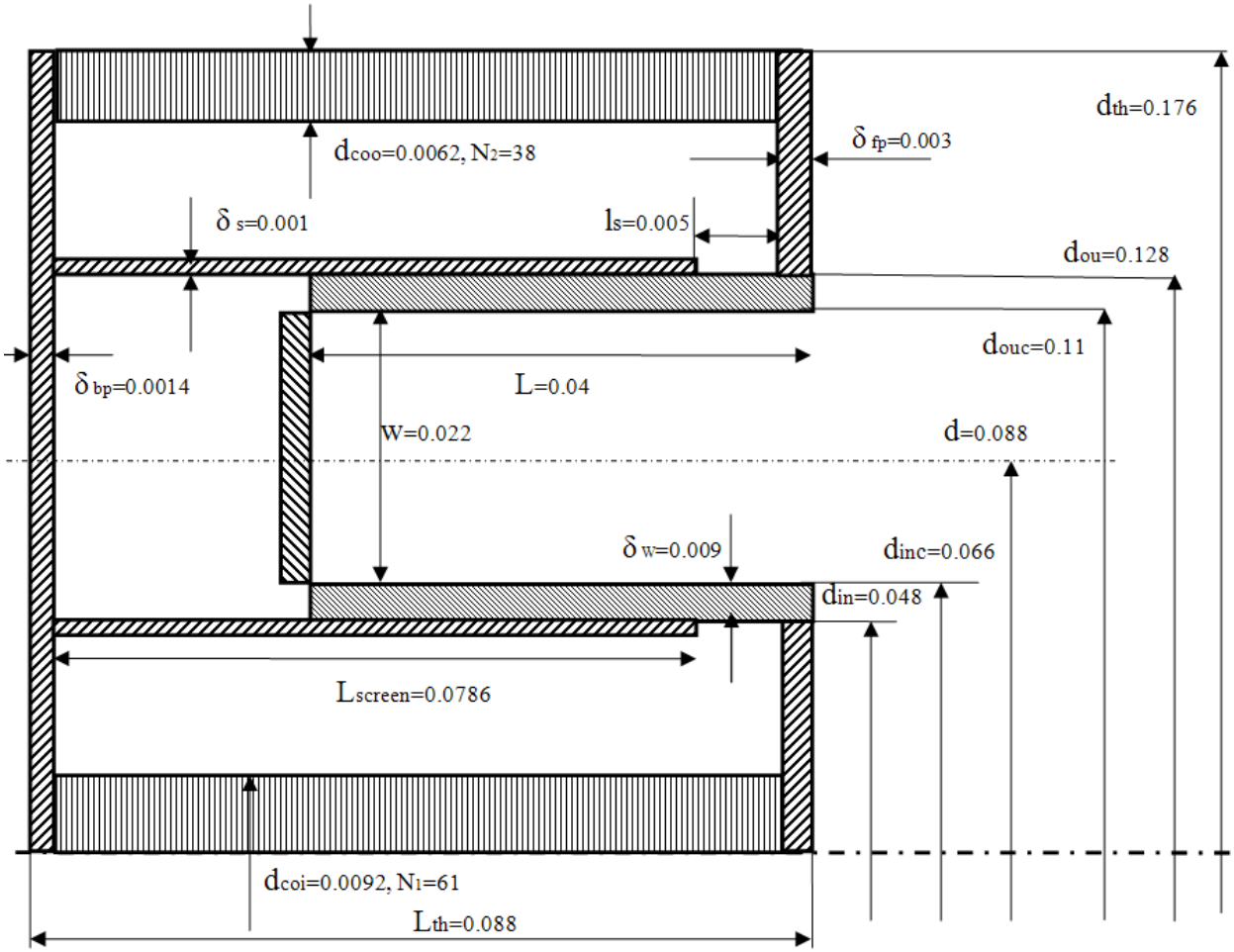

Figure 15. Schematic view of the designed thruster.

IV. Conclusion

There are still many questions about the physics of the Hall thruster including the full description of the plasma dynamics and the physics of the plasma instabilities. The design algorithm presented here shows that experimental data for a detailed design of a thruster is vital. The lifetime criterion is the most important parameter which must be checked before proceeding for magnetic field's calculations. In addition it is clear that if the magnetic field in the thruster changes with time then the Kirchhoff's solution must be reconsidered.

References

[1]Kim, V., Kozubsky, K. N., Murashko, V. M., and Semenkin, A. V., "History of the Hall Thrusters Development in USSR," Proceeding of the 30th International Electric Propulsion Conference, Florence, Italy, 2007, pp. 07-142.

[2]Kozubskii, K. N., Murashko, V. M., Rylov, Yu. P., Trifonov, Yu. V., Khodnenko, V. P., Kim, V., Popov, G. A., and Obukhov, V. A., "Stationary Plasma Thrusters Operate in Space," The 30th Anniversary of SPT Operation in Space, Plasma Physics Reports, Vol. 29, No. 3, 2003, pp.251-266.

[3]Goebel, D. M., Katz, I., "Fundamentals of Electric Propulsion, Ion and Hall Thrusters," JPL Space Science and Technology Series, John Willy and Sons, Inc., Hoboken, New Jersey, 2008, chap.7.

[4]Zhurin, V. V., Kaufman, H. R., Robinson, R. S., "Review Article: Physics of closed drift thrusters," Plasma Sources Sci. Technol. 8 (1999) R1–R20.

[5]Bugrova, A. I., Kim, V. P., Maslennikov, N. A., Morozov, A. I., "Physical Processes and Characteristics of Stationary Plasma Thrusters with Closed Electrons Drift, " Proceeding of the 22nd International Electric Propulsion Conference, Viareggio, Italy, 1991, pp. 91-079.

[6]Kim, V., "Main Physical Features and Processes Determining the Performance of Stationary Plasma Thrusters," Journal of Propulsion and Power, Vol. 14, No. 5, 1995, pp.736-743.

[7]Arkhipov, B. A., Veselovzorov, A. N., Gavryushin, V. M., Khartov, S. A., Kim, V., Kozlov, V. I., Maslennikov, V. I., Morozov, A. I., Murashko, V. M., Pokrovski, I. B., "Development and Investigation of Characteristics of Increased Power SPT Models," Proceeding of the 23rd International Electric Propulsion Conference, Seattle, USA, 1993, pp. 93-222.

[8]Belan, N. V., Kim, V. P., Sevruk, D. D., "The Engendering Method of SPT Calculation," Kharkov Aviation Institute, 1980 (in Russian).

[9]Belan, N. V., Kim, V. P., Oransky, A. I., Tikhonov, V. B., "Stationary Plasma Thrusters," Kharkov Aviation Institute, 1989 (in Russian).

[10]Hofer, R. R., "Development and Characterization of High-Efficiency, High-Specific Impulse Xenon Hall Thrusters," Ph.D. Thesis, University of Michigan, 2004.

[11]Warner, N. Z., "Theoretical and Experimental Investigation of Hall Thruster Miniaturization," Ph.D. Thesis, Massachusetts Institute of Technology, 2007.